Chapter 8

Studies on monolayer of functionalized gold particles

8.1 Introduction

There are numerous reports suggesting the applications of nanometer sized metal particles [1, 2]. They find potential applications in fabricating superlattices whose optical and electronic properties are tunable. One of the important parameters determining the properties of such materials is the interparticle separation. Other parameters are charging energy of the particles, strength of interaction between the particles and the symmetry of the lattice [3–6]. These particles show the quantum coupling. The coupling of the electronic wavefunctions associated with each particle depends on the interparticle separation. Heath and coworkers have observed an insulator to metal (MI) transition during the compression of a monolayer of the functionalized silver nanoparticles (quantum dots) at the air-water (A-W) interface [7, 8]. There are numerous reports on the study of Langmuir monolayer of purely hydrophobic functionalized metal particles [7–11]. The important criterion for the formation of stable Langmuir monolayer at the A-W interface is that the molecules should be amphiphilic in nature with a proper balance between the hydrophilic and hydrophobic parts of the molecule [12]. Brown *et al*. [13] have reported a TEM study on the monolayer of amphiphilic gold particles transferred on the carbon and copper grids. Their studies has revealed a hexagonal ordering of the gold particles in the film. However, there is no surface manometry studies of the Langmuir monolayer of such particles.

In this chapter we describe our study on the monolayer properties of amphiphilic functionalised gold particles.

8.2 Experimental

The amphiphilic functionalized gold particle (organometallic) was synthesized in the chemistry laboratory of our Institute [14]. The more details about the particle are given in Appendix A. The structure is shown in Figure 8.1. The presence of terminal -OH group gives an amphiphilic nature to the particle. The transmission electron microscope (TEM) images

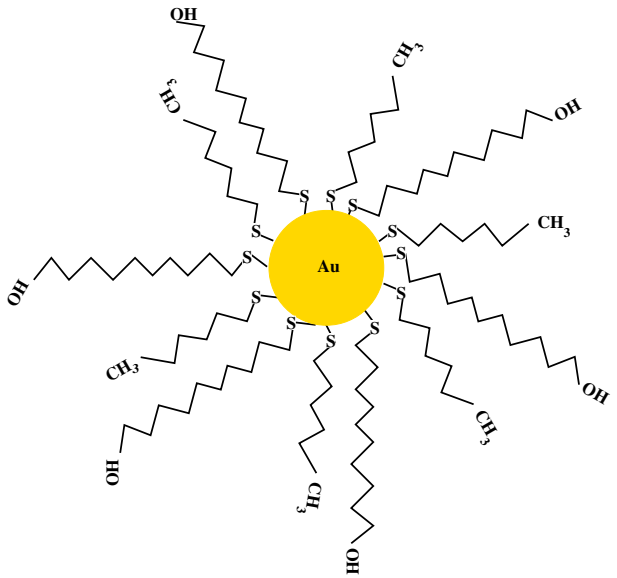

Figure 8.1: Structure of the functionalized gold particle.

were obtained using JOEL JEM-200CX. The sample of the functionalized gold particle (FGP) dissolved in methanol, was spread on the carbon evaporated copper grid, and the image was scanned after 60 minutes in an operating voltage of 120 kV. To form the Langmuir monolayer, the FGP was dissolved in 80% toluene and 20% methanol (HPLC grade) to obtain a solution of 0.1 mg/ml. The solution was spread on the ultrapure ion-free water and about 45 minutes time was allowed for the solvent to evaporate from the water surface. The compression speed was maintained at 10.7 (nm^2/molecule)/minute. The temperature of the subphase was maintained by circulating water inside the chamber of the trough using a thermostat (Julabo, F25-MV). The other details of surface manometry and Brewster angle

microscope (BAM) experiments are similar as discussed in the previous chapters. A single layer of the FGP in different phases were transferred on gold substrates by the Langmuir-Blodgett (LB) technique. The transfer ratios during LB deposition were 1±0.1. The details of the substrate preparation are discussed in chapter 5. The grazing angle reflection absorption infrared spectroscopy (RAIRS) was carried out using a home built setup (angle of reflection = 86°) and a FTIR spectrometer having a resolution of 4 cm^{-1}. The details of RAIRS are described in Appendix B.

8.3 Results

The size of the FGP was determined using (TEM). We find that the particle core had a mean diameter of 5.5 nm (Figure 8.2). Assuming the organic ligands (mercapto-1-undecanol and hexanethiol) to be uniformly covering the gold particle, the diameter of the FGP for the fully stretched ligands was estimated to be 8.4 nm. Therefore, the cross-sectional area of each particle was 55.4 nm^2.

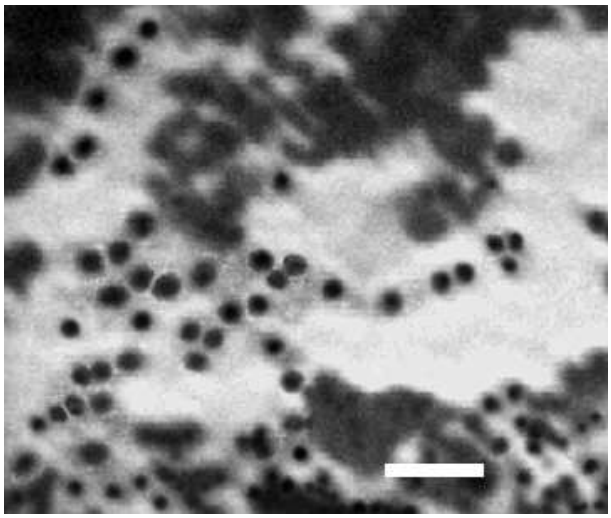

Figure 8.2: The transmission electron microscope image of the FGP. The black circles represent the core of the FGP. It has a mean diameter of 5.5 nm. The scale bar represents 25 nm.

The surface pressure (π) - area per molecule (A_m) isotherms of the FGP at different temperatures are shown in Figure 8.3. The isotherms at low temperatures (<28 °C) show a lift-off area at around 120 nm^2. Then the surface pressure rises slowly (region I). The

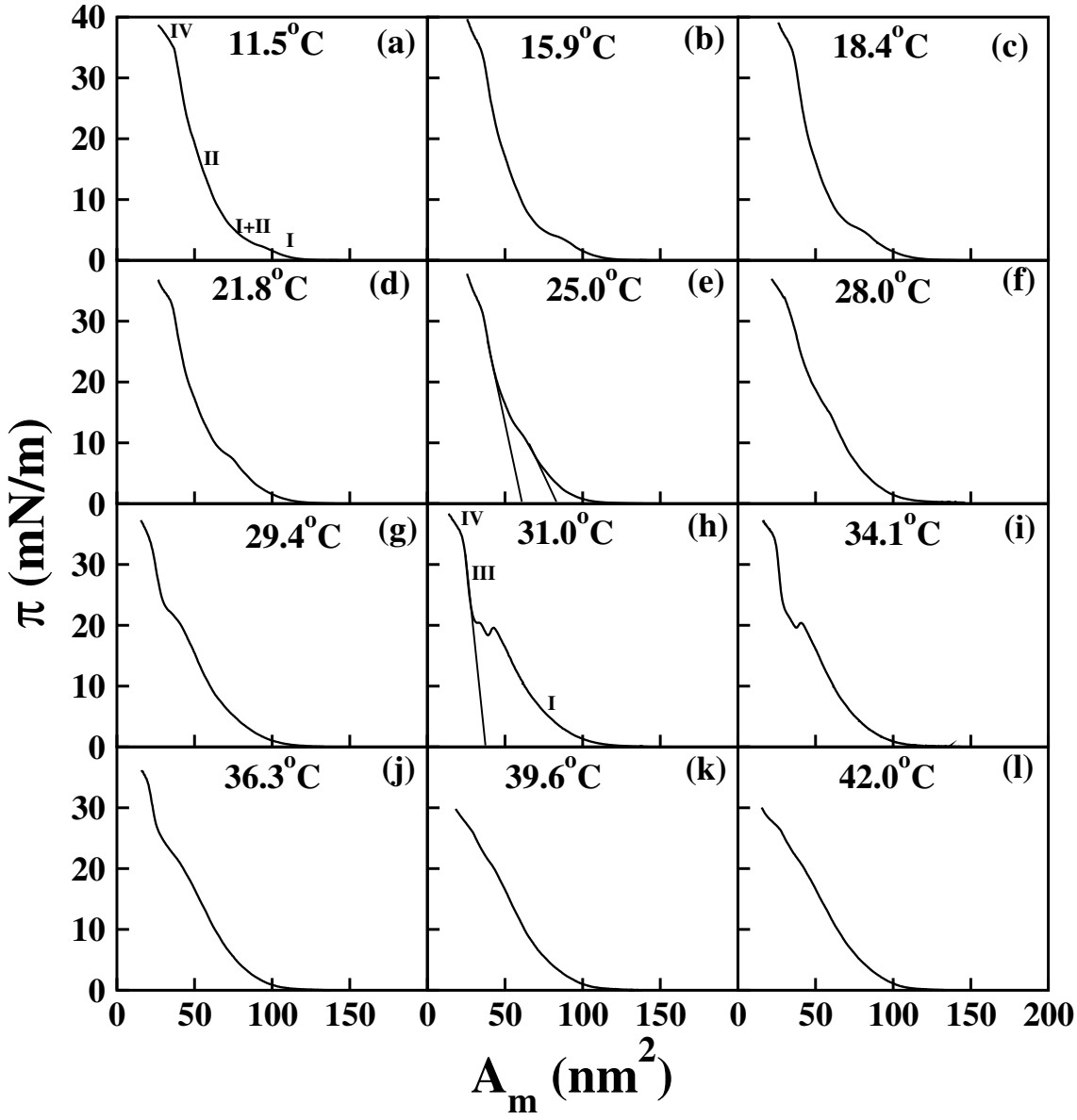

Figure 8.3: Surface pressure (π) - area per molecule (A_m) isotherms of functionalized gold particle (FGP) monolayer at different temperatures. The different regions of the isotherms representing different phases are labeled as I, II, III and IV, respectively. These are shown in the figures (a) and (h). The straight lines are drawn in the figures (e) and (h) to depict an extrapolation of the regions of the isotherm to the zero surface pressure.

isotherms show a small plateau which may correspond to a region of the coexisting phases (region I+II). Around 75 nm^2, the surface pressure starts rising gradually to higher values (region II). The extrapolated area per molecule of the region I and region II are around 85 and 61 nm^2, respectively, as shown in Figure 8.3(e). A relative surface density of the phase corresponding to region II with respect to region I is 1.4 (85 nm^2/61 nm^2) at 25 °C. The

isotherms show a gradual collapse with a small change in the slope of the isotherm (region IV). With the increase in temperature, the surface pressure corresponding to the onset of the plateau increases. On the other hand, the range of the plateau decreases with increasing temperature. The plateau vanishes slightly above 28 °C. These are the characteristic features of first order phase transition [15]. For temperature range of 29 to 36°C, the isotherms show a rise in surface pressure on decreasing A_m which correspond to the region I. At around 45 nm^2, the isotherms show a collapse-like feature. After the collapse, the surface pressure rises steeply. The steep region of the isotherm is denoted by region III. The extrapolated area per molecule, obtained from the region III, was around 31.3 nm^2. The phase corresponding to region III collapses on further decrease in A_m. The region III shows a vanishing trend on further increase in the temperature. Above 36.3 °C, the isotherms show only the phase corresponding to the region I.

We have observed the monolayer of FGP using a Brewster angle microscope at different temperatures. The BAM images at a temperature of 25 °C are shown in Figure 8.4. At a very large A_m (Figure 8.4(a)), the image shows a coexistence of dark (gas phase) and gray region. On compression, the dark region vanishes at the expense of the gray region yielding an uniform gray background (Figure 8.4(b)). This corresponds to a phase indicated by the region I in the isotherm. On further compression, some bright domains were seen to be growing in the gray background (Figure 8.4(c)) . This was observed in the coexisting region of the isotherm indicated by the region I+II. On compression, the bright domains grow in size and merge to yield a very uniform bright background (Figure 8.4(d)). This corresponds to a phase indicated by the region II in the isotherms. The monolayer collapses on further compression. In the collapsed state, a few dark spots were seen in the folded-like bright texture (Figure 8.4(e)).

The BAM images of the monolayer of FGP at a temperature of 31.0 °C are shown in Figure 8.5. The image at a very large A_m shows a coexistence of dark and gray regions (Figure 8.5(a)). On compression, the dark region disappears leading to an uniform gray texture. The uniform gray texture corresponds to the phase indicated by the region I in the

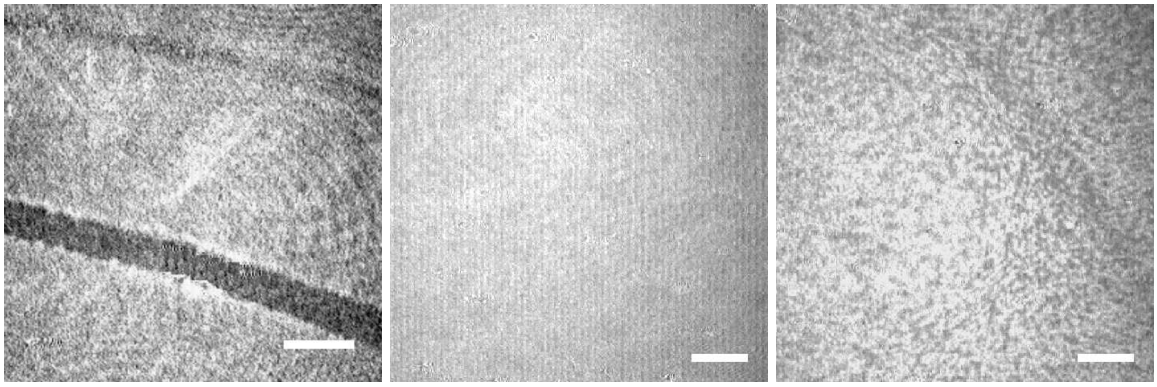

(a) 250.0 nm^2 (b) 75.0 nm^2 (c) 61.3 nm^2

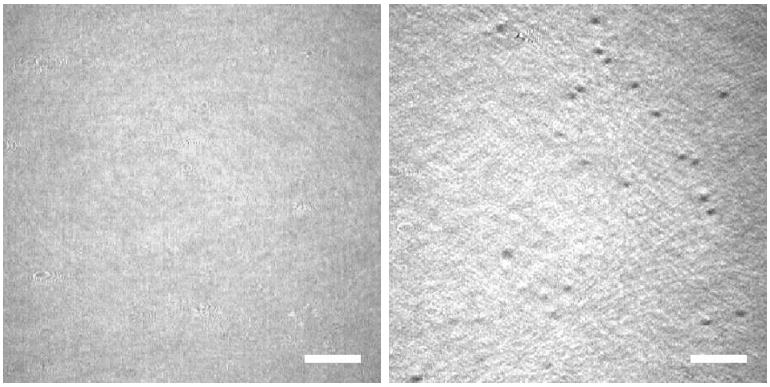

(d) 47.5 nm^2 (e) 30.0 nm^2

Figure 8.4: BAM images of FGP monolayer on ion-free water at a temperature of 25°C. The images were captured at an A_m shown below the respective images. (a) shows a coexistence of dark (gas phase) and gray region at a very large A_m. (b) shows a uniform gray background representing a homogeneous phase corresponding to the region I. (c) shows bright domains growing over the gray background. This corresponds to the coexisting region indicated by I+II in the isotherms. (d) shows a very uniform bright texture corresponding to the phase indicated by region II in the isotherms. (e) shows a texture corresponding to the collapse of the monolayer. The image shows a few dark spots in a folded-like bright texture. This was observed in the region indicated by IV in the isotherm. The scale bar represents 500 μm.

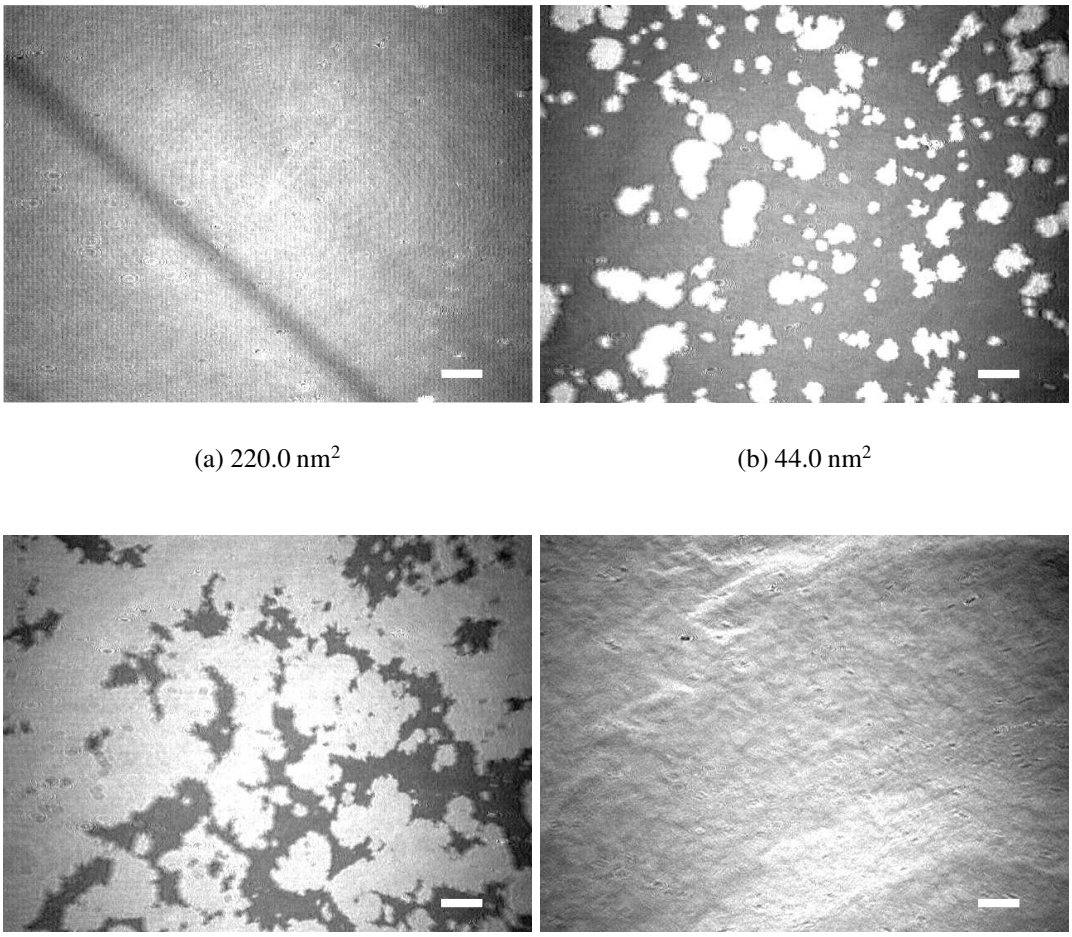

(a) 220.0 nm^2 (b) 44.0 nm^2

(c) 36.5 nm^2 (d) 14.2 nm^2

Figure 8.5: BAM images of the FGP monolayer on the ion-free water at a temperature of 31°C. (a) shows a coexistence of dark (gas) and a gray region at a very large A_m. (b) shows some brighter domains growing on the gray background. (c) shows much larger area of the brighter domains in the gray background. (b) and (c) were observed in the collapsed-like region of the isotherm (Figure 8.3(h)). (d) shows a collapsed state. The collapsed state reveals a folded-like texture. This was observed in the region indicated by IV in the isotherm. The scale bar represents 500 μm.

isotherm. On further compression, some brighter domains grow on the gray background (Figure 8.5(b)). The brighter domains continue to grow on compression (Figure 8.5(c)). The patterns shown in Figures 8.5(b and c) were observed in the collapse-like region of the isotherm. The brighter domains merge to yield an uniform texture. This phase corresponds to the region III shown in the isotherm. On further compression, the film collapses showing a folded-like texture (Figure 8.5(d)) in the BAM image. This corresponds to the phase indicated by the region IV in the isotherm. We designate the phases corresponding to the regions I, II and III of the isotherms as L_{1d}, L_{1o} and B_{1o}, respectively.

We have transferred the LB films of FGP at different target surface pressures (π_c) corresponding to the different phases. The LB films were analyzed by RAIRS. The reflection absorption spectrum of the transfered monolayer was taken immediately after the transfer. This is shown in Figure 8.6. We have analysed the peaks corresponding to the asymmetric

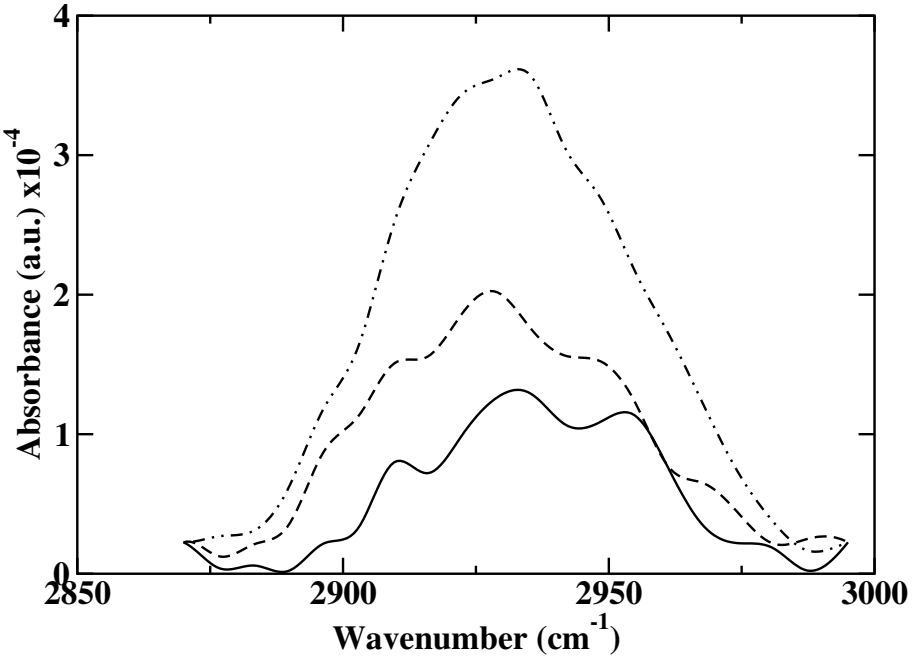

Figure 8.6: Reflection absorption infrared spectra for the LB films of FGP on gold substrate deposited at the different target surface pressures corresponding to different phases. The vibration band represents the stretching mode of the alkyl chains (CH) of FGP. The solid (−) and the dashed (−−) lines represent the spectra for the LB films transfered at a temperature of 25.0 °C and at the surface pressures of 4 and 20 mN/m, respectively. The spectra correspond to the L_{1d} and L_{1o} phases, respectively. The dotted-dashed line ($\cdots-\cdots$) represents the spectrum of the LB film transfered at a temperature of 31.0 °C and at a surface pressure of 27 mN/m. The spectrum corresponds to the B_{1o} phase.

stretching of the alkyl chains (CH) of the funtionalised gold particles. The symmetric stretch for the -CH_2 and -CH_3 peaks could not be resolved in the spectrum obtained from our setup. The IR spectrum of the bulk sample also showed relatively weak peaks for the -CH_2 and -CH_3 symmetric stretching. The asymmetric stretch for both the groups were not well separated. Nonetheless, they together contribute to a well defined peak from 2890-2988 cm^{-1}. The IR spectra for the asymmetric stretching of the -CH_2 and -CH_3 are shown for the L_{1d}, L_{1o} and B_{1o} phases. The area under the peak was computed. It gives the integrated absorbance for the characteristic band. For the L_{1d}, L_{1o} and B_{1o} phases, the integrated absorbance $A_{L_{1d}}$, $A_{L_{1o}}$ and $A_{B_{1o}}$ were found to be 0.0065, 0.0083 and 0.0164 (a.u.), respectively.

8.4 Discussion

The region corresponding to I in the isotherms show a large value of lift-off area per molecule (~110 nm^2 at 25 °C). This region displays a fluid-like and an uniform gray texture in the BAM images (Figure 8.4(a)). The maximum value of elastic modulus in this phase, calculated from the isotherm at 18.4 °C, was merely 17.6 mN/m. The extrapolated area per molecule in this phase yields a value equal to 85 nm^2. The phase corresponding to the region I in the isotherms can be considered as a low density disordered liquid (L_{1d}) phase. On compression, the L_{1d} phase transforms to another phase, as indicated by the region II in the isotherms through a first order transition. The coexistence of the phases were indicated by the plateau in the isotherms (region I+II). The extrapolated area per molecule of the phase, indicated by the region II, yields a value of 61 nm^2. This value approximately corresponds to the average size of the FGP determined from the TEM images. Also, the phase in the region II is about 1.4 times denser than that of L_{1d} phase. The BAM images in the region of coexisting phases (indicated by I+II in the isotherms) reveal a liquid-like bright domains growing on the L_{1d} phase (Figure 8.4(c)). On compression, the bright domains grow and finally yield a very uniform bright texture (Figure 8.4(d)). This corresponds to the phase indicated by the region II in the isotherms. The BAM image in this region does not reveal any optical anisotropy suggesting the phase to be an isotropic liquid phase. The maximum

value of in-plane elastic modulus, calculated from the isotherm at 18.4 °C in this region, was found to be 48.4 mN/m. This value is smaller as compared to the condensed phase of stearic acid or that of cholesterol. Hence we interpret, the phase corresponding to the region II to be as a liquid-like (L_{1o}) phase which is denser than L_{1d} phase. With increasing temperature, the range of the plateau corresponding to the coexistence of L_{1d} and L_{1o} phase decreases and finally vanishes above 28.0 °C. We have estimated the critical temperature (t_c) by determining the range of coexisting region as a function of temperature. We estimate the value of t_c to be equal to 28.4 °C. Above t_c, the BAM image (Figure 8.5(a)) shows a gray texture at a large A_m representing the L_{1d} phase. On compression, the L_{1d} phase destabilizes and gives rise to another phase corresponding to region III in the isotherms. The extrapolated area per molecule in this region of the isotherm yields a value of 31 nm^2. This value is about half compared to that of L_{1o} phase. We suggest that this phase may be a bilayer of L_{1o} phase. We have designated this phase as, B_{1o}. The BAM images in the Figure 8.5(b and c) show the growth of the bilayer (brighter domains) on compression. The fully grown B_{1o} phase displays a brighter uniform texture. The B_{1o} phase also collapses on compression. The BAM image in the collapsed state shows a folded-like texture (Figure 8.5(d)). The folding of the monolayer in the collapsed state have also been observed in other systems [16–19].

We have carried out the RAIRS experiments to determine the relative surface density of the molecules and the thickness of the films in different phases. Absorbance is proportional to the thickness and the surface density of the sample. For the phase α, the absorbance (A_α) can be written as

$$A_\alpha = 2\epsilon\rho_\alpha \frac{d_\alpha}{cos(\theta)} \tag{8.1}$$

where ϵ is absorptivity, ρ_α is the surface density of the molecules in the phase α, d_α is the thickness of the film in the phase α and θ is the angle of incidence. The factor 2 comes due to the reflection from the substrate. The ratio of the absorbance in the phases α and α' ($R_{\alpha,\alpha'}$) can be written as

$$R_{\alpha,\alpha'} = \frac{A_\alpha}{A_{\alpha'}} = \frac{\rho_\alpha d_\alpha}{\rho_{\alpha'} d_{\alpha'}} \tag{8.2}$$

Assuming the thickness of the monolayer in L_{1d} and L_{1o} phases to remain the same, the

difference in the integrated absorbance values in the two phases can be attributed to the difference in surface density. Hence, from Equation 8.2, the $R_{L_{1o},L_{1d}}$ will yield the relative surface density of the phase L_{1o} with respect to the phase L_{1d}. The integrated absorbance values in the L_{1o} and L_{1d} phases were found to be 0.0083 and 0.0065, respectively. This yields the $R_{L_{1o},L_{1d}}$ value to be 1.28 which suggests that the surface density of the L_{1o} phase is about 1.28 times greater than that of L_{1d} phase. From the π-A_m isotherm obtained at 25 °C, we find the surface density of L_{1o} phase to be 1.4 times greater than that of L_{1d} phase. This shows that the values obtained from the π-A_m isotherms and RAIRS experiments are nearly in agreement. The slight difference in the values can be attributed to the non-uniformity in the LB films due to surface roughness of the gold substrates on which the films were deposited.

Similarly, assuming the surface density of the B_{1o} phase to be same as that of the L_{1o} phase, the difference in the integrated absorbance values in these phases can be attributed to the difference in the film thickness. In such case, the Equation 8.2 will yield a relative thickness of the films in the two phases. The integrated absorbance values in the B_{1o} and L_{1o} phases were found to be 0.0083 and 0.0164, respectively which yields $R_{B_{1o},L_{1o}}$ to be 1.97. This is nearly two indicating that the B_{1o} phase is a bilayer of L_{1o} phase.

Based on our surface manometry, microscopy and spectroscopy studies, we have constructed a phase diagram shown in Figure 8.7. It has to be pointed that since the particle is spherical in shape, the phase transitions are mainly occuring due to the change in interparticle distances and the ordering among the organic mercapto-1-undecanol and hexanethiol ligands. The phase diagram also shows that the surface pressure corresponding to the L_{1d} to L_{1o} transition increases with increasing temperature. The positive slope ($d\pi/dt$) of the L_{1d}-L_{1o} transition curve indicates a decrease in the entropy during the transition [15]. Hence, we suggest that the phase L_{1o} is more ordered as compared to that of L_{1d} phase.

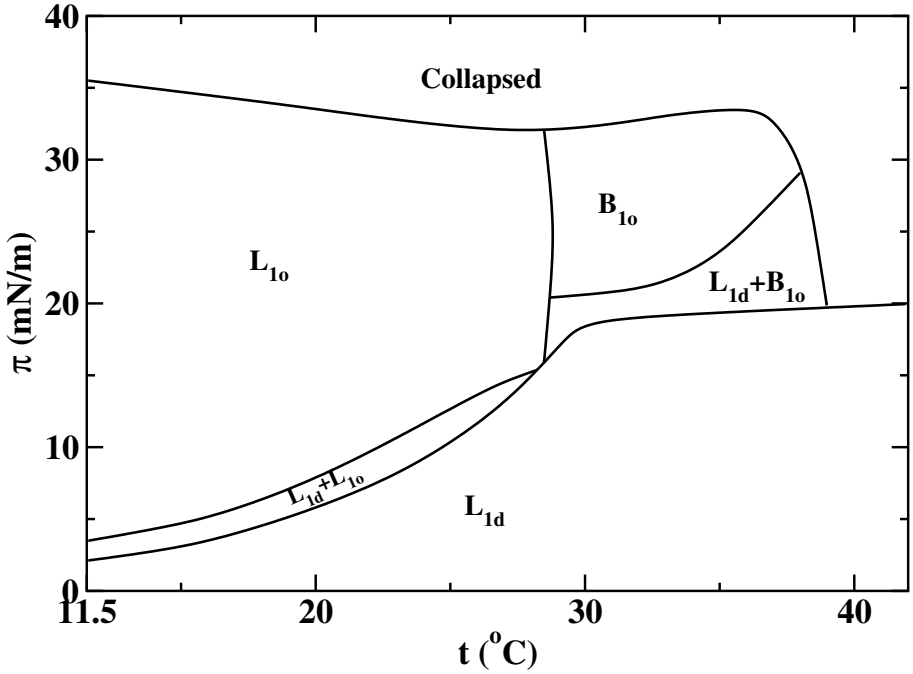

Figure 8.7: Phase diagram showing the monolayer phases of the functionalized gold particles. Here, t represents the temperature of the subphase and π represents the surface pressure. The symbols L_{1d}, L_{1o} and B_{1o} represent low density disordered liquid, high density ordered liquid and bilayer of L_{1o} phases, respectively. The L_{1d} and gas phase coexistence was seen even at very large A_m and zero surface pressure.

8.5 Conclusions

Though there are numerous reports on the Langmuir monolayer of the hydrophobic functionalized metal particles, there are only a few reports on the amphiphilic metal particles. We have obtain a stable Langmuir monolayer of the amphiphilic functionalized gold particles. The monolayer of the particles shows variety of interesting two-dimensional phases. It exhibits low density disordered liquid (L_{1d}) phase, high density ordered liquid (L_{1o}) phase, bilayer of L_{1o} phase (B_{1o} phase) and a collapsed state. At low temperature, the isotherms reveal a transition from L_{1d} to L_{1o} phase accompanied by a coexistence of the phases. Above the critical temperature of 28.4 °C, the monolayer shows L_{1d} and B_{1o} phases. Above 37 °C, B_{1o} phase disappears and the monolayer shows only L_{1d} phase.

Bibliography

[1] M-C. Daniel and D. Astruc, Chem. Rev. **104**, 293 (2004).

[2] M. Burst and C. J. Kiely, Colloids Surf. A **202**, 175 (2002).

[3] P. Zhang and T. K. Sham, Phys. Rev. Lett. **90**, 245502 (2003).

[4] L. P. Kouwenhoven, F. W. Hekking, B. J. van weeb, C. J. P. M. Harmans, C. E. Timmering, and C. T. Foxon, Phys. Rev. Lett. **65**, 361 (1990).

[5] C. I. Duruoz, R. M. Clarke, C. M. Marcus, and J. S. Harris, Jr., Phys. Rev. Lett. **74**, 3237 (1995).

[6] A. J. Rimberg, T. R. Ho, and J. Clarke, Phys. Rev. Lett. **74**, 4714 (1995).

[7] C. P. Collier, R. J. Saykally, J. J. Shiang, S. E. Henrichs, and J. R. Heath, Science **277**, 1978 (1997).

[8] G. Markovich, C. P. Collier, and J. R. Heath, Phys. Rev. Lett. **80**, 3807 (1998).

[9] J. R. Heath, C. M. Knobler, and D. V. Leff, J. Phys. Chem. **101**, 189 (1997).

[10] A. Swami, A. Kumar, P. R. Selvakannan, S. Mandal, and M. Sastry, J. Colloid Interface Sci. **260**, 367 (2003).

[11] I. A. Greene, F. Wu, J. Z. Zhang, and S. Chen, J. Phys. Chem. B **107**, 5733 (2003).

[12] G. L. Gaines, Jr., *Insoluble Monolayers at Liquid-Gas Interfaces* (Wiley-Interscience, New York, 1966).

[13] J. J. Brown, J. A. Porter, C. P. Daghlian, and U. J. Gibson, Langmuir **17**, 7966 (2001).

[14] Sandeep Kumar (To be published)

[15] H. B. Callen, *Thermodynamics And An Introduction To Thermostatistics*, (Second Edition, Wiley,1985).

[16] C. Liu and A. J. Bard, Nature (London) **418**, 162 (2002).

[17] W. Lu, C. M. Knobler, R. F. Bruinsma, M. Twardos, and M. Dennin, Phys. Rev. Lett. **89**, 146107 (2002).

[18] M. M. Lipp, K. Y. C. Lee, D. Y. Takamoto, and A. J. Waring, Phys. Rev. Lett. **81**, 1650 (1998).

[19] A. Gopal and K. Y. C. Lee, J. Phys. Chem. B **105**, 10348 (2001).